Journal of Medicinal Chemistry

Article

pubs.acs.org/jmc

Investigation of the Noncovalent Binding Mode of Covalent Proteasome Inhibitors around the Transition State by Combined Use of Cyclopropylic Strain-Based Conformational Restriction and Computational Modeling

Shuhei Kawamura,[†] Yuka Unno,[§] Motohiro Tanaka,[∥] Takuma Sasaki,[∥] Akihito Yamano,[⊥] Takatsugu Hirokawa,[#] Tomoshi Kameda,[#] Akira Asai,[§] Mitsuhiro Arisawa,[†] and Satoshi Shuto*,[†,‡]

[†]Faculty of Pharmaceutical Sciences and [‡]Center for Research and Education on Drug Discovery, Hokkaido University, Kita-12, Nishi-6, Kita-ku, Sapporo 060-0812, Japan

[§]Graduate School of Pharmaceutical Sciences, University of Shizuoka, Yada, Shizuoka 422-8526, Japan

[∥]School of Pharmacy, Aichi Gakuin University, 1-100 Kusumoto-cho, Chikusa-ku, Nagoya 464-8650, Japan

[⊥]Rigaku Corporation, X-ray Institute, 3-9-12 Matsubara-cho, Akishima, Tokyo 196-8666, Japan

[#]Computational Biology Research Center (CBRC), National Institute of Advanced Industrial Science and Technology (AIST), 2-4-7 Aomi, Koutou-ku, Tokyo 135-0064, Japan

Supporting Information

ABSTRACT: To develop potent covalent inhibitors, the noncovalent interactions around the transition state to form covalent bonding should be optimized because the potency of the inhibitor can be depending on the energy of the transition state. Here, we report an efficient analysis of the noncovalent binding mode of a potent covalent proteasome inhibitor **3a** around the transition state by a combined use of the chemical approach, i.e., the cyclopropylic strain-based conformational restriction, and the computational docking approach. Furthermore, we calculated the binding energy of a series of salinosporamide derivatives in the predicted noncovalent complex around the transition state with the simulation model of proteasome constructed in this study, which was well correlated to their pIC_{50}. Thus, the proposed docking methods to predict the noncovalent binding mode around the transition state of covalent inhibitors will be helpful toward the development of covalent inhibitors.

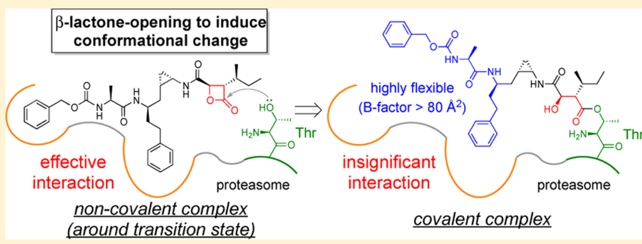

INTRODUCTION

Much attention has been focused on covalent inhibitors of proteins due to their strong and prolonged inhibitory effects based on the stable covalent bonding.[1] Many covalent inhibitors are useful as clinical drugs[1] and also as tools for investigating biological pathways.[2] Even if an inhibitor binds covalently to its target protein, it should first be recognized by its target via noncovalent interactions to form a reversible noncovalent complex (P·I). After that, it reacts with the reacting group of the target protein via transition state (P···I) to form the covalent complex (P−I)[1a] as shown in Figure 1.

Accordingly, the potency of covalent inhibitors can be significantly affected by their binding affinity for the target protein in the noncovalent binding mode, especially around its transition state to form covalent bonding. Therefore, to design optimized covalent inhibitors, it is desirable to know the noncovalent binding mode of the lead inhibitor around the transition state, which can be the "bioactive conformation" of covalent inhibitors.

X-ray crystallographic structures of inhibitors in complex with their targets are often effectively used for designing further active inhibitors.[3] For the design of covalent inhibitors, however, the X-ray structure of the complex might not be so helpful compared with the design of noncovalent inhibitors because conformation of the covalent inhibitors in the binding site can be significantly changed along with the covalent bond formation. In such cases, the noncovalent binding mode around the transition state cannot be effectively predicted by the X-ray crystallographic analysis. Thus, it is difficult to analyze the noncovalent binding mode of covalent inhibitors around the transition state for the optimization process of covalent inhibitors.

In recent years, proteasome inhibitors have been extensively studied from the viewpoint of antitumor drug discovery.[4] Because the systematic degradation of intracellular proteins by proteasome is essential for cellular functions such as cell cycle progression,[5] signal transduction,[6] and endoplasmic reticulum-associated protein degradation (ERAD),[7] proteasome inhibition causes cell cycle arrest and induces apoptosis.[4a,b] In fact, the proteasome inhibitors bortezomib and carfilzomib were approved by FDA for the treatment of multiple myeloma,[8] and

Received: April 15, 2013
Published: June 25, 2013

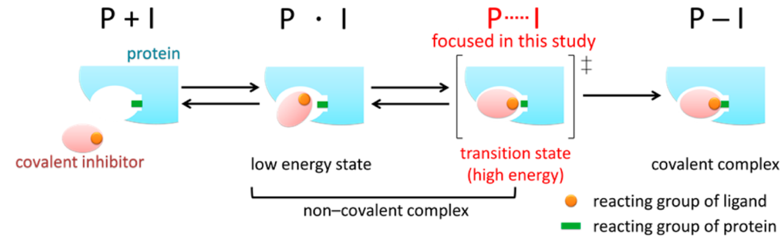

Figure 1. Inhibitory mechanism of covalent inhibitors.

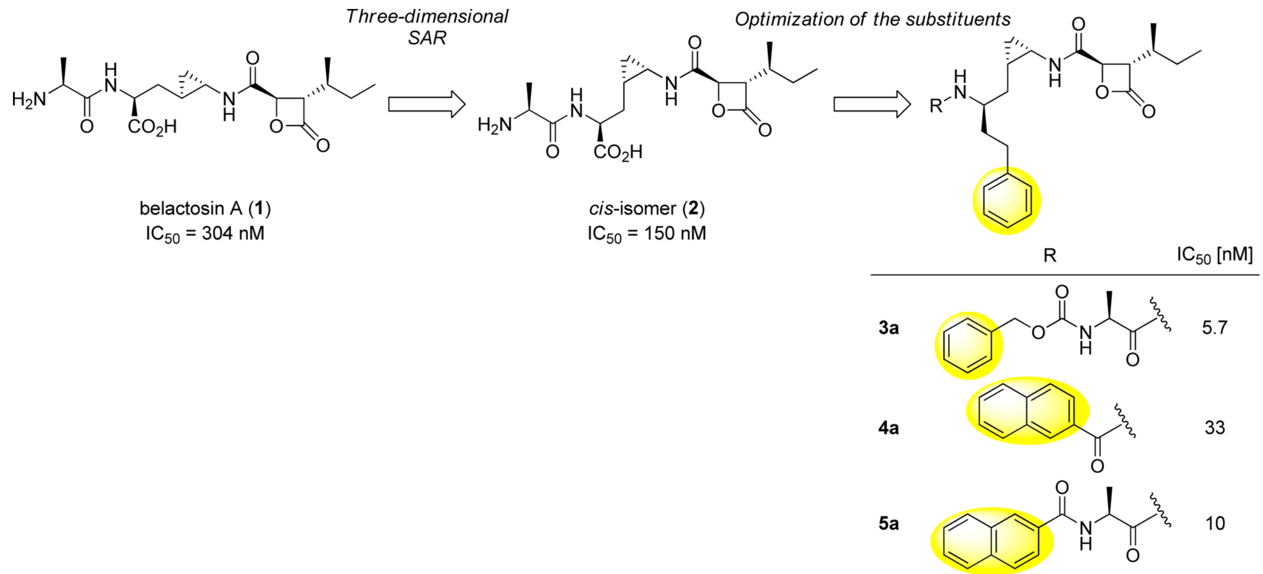

Figure 2. Development of potent proteasome inhibitors using belactosin A as a lead by the stereochemical diversity-oriented strategy.

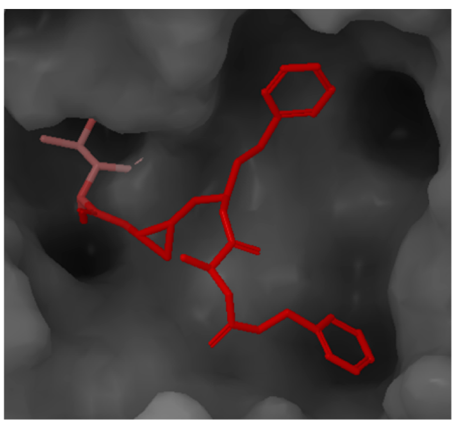

Figure 3. X-ray crystallographic analysis of **3a** in complex with proteasome. The structure of **3a** was colored according to its *B*-factor value, in which the areas with low *B*-factors are colored blue and the areas with high *B*-factors are colored red.

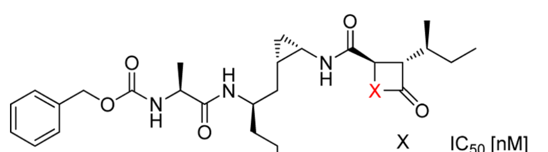

	X	IC_{50} [nM]
3a	O	5.7
3a'	NH	> 10000

Figure 4. The structure and proteasome inhibitory activity of β-lactam congener **3a′**.

several proteasome inhibitors are currently in clinical trials.[4b] Notably, all of these inhibitors bind covalently to proteasome, showing the effectiveness of covalent inhibitors as anticancer agents.

Belactosin A (**1**) is a naturally occurring tripeptide identified as a proteasome inhibitor by Asai and co-workers.[9] It inhibits proteasome covalently by acylating the active site Thr residue via ring-opening of its β-lactone moiety.[10] We previously developed highly potent proteasome inhibitors **3a**−**5a** by the three-dimensional structure−activity relationship (SAR) of belactosin A[11] and subsequent optimization studies (Figure 2).[12] These studies revealed that the two hydrophobic moieties (yellow in Figure 2) on the left side of the molecules are important for the high potency of **3a**−**5a**, compared with the lead **2**.

We also analyzed the X-ray crystal structure of **3a** in complex with proteasome,[12b] but, the *B*-factors, which represent smearing of atomic electron densities around their equilibrium positions due to thermal motion and positional disorder,[13] of **3a** were unexpectedly high; the average ligand *B*-factor was greater than 80 Å^2, especially in the region containing the two hydrophobic moieties (Figure 3). This suggests that, in the covalent complex, the region containing the two hydrophobic moieties of **3a** is highly flexible and would not interact effectively with proteasome, while the two moieties are clearly necessary for high inhibitory activity. This contradictory result indicates that the region containing two hydrophobic moieties effectively interacts with proteasome to facilitate noncovalent complex formation and/or covalent bond formation. Once the covalent bond is formed, the conformation of **3a** would be significantly

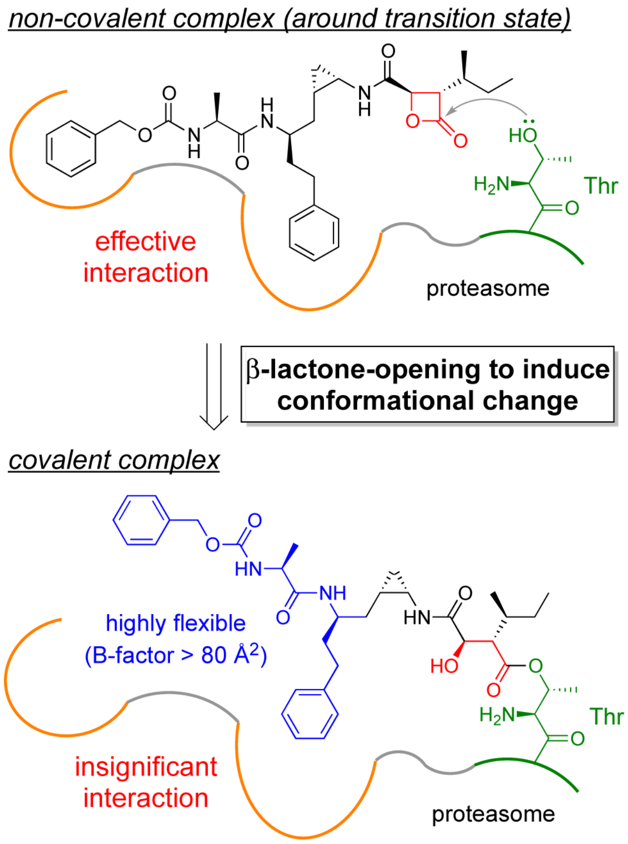

Figure 5. Plausible binding mode change of **3a** with proteasome before and after covalent bond formation.

altered due to its strained β-lactone-opening, which would weaken the interaction of the two hydrophobic moieties with proteasome.

To further analyze the contribution of noncovalent interactions in these inhibitors, the β-lactam congener **3a′** was synthesized and evaluated its proteasome inhibitory potency (Figure 4). Because the reactivity of β-lactam is much lower than the corresponding β-lactone, covalent bond formation should be significantly retarded in **3a′**. In stark contrast to **3a**, the β-lactam congener **3a′** showed no proteasome inhibitory activity (IC_{50} > 10000 nM). This clearly suggests that, in these compounds, the noncovalent complex prior to covalent bond formation is not stable enough to exhibit proteasome inhibitory activity by itself and proteasome inhibitory activity of belactosin derivatives is predominantly owing to their covalent bond formation ability. Thus, the region containing the two hydrophobic moieties of **3a** should effectively interact with proteasome in its transition state to facilitate covalent bond formation.

Therefore, to effectively optimize the noncovalent interactions of **3a** with proteasome by further structural modifications, the analyses of the noncovalent binding mode of **3a** with proteasome around the transition state are necessary (Figure 5).

The organic chemistry-based approach by synthesizing conformationally restricted analogues of a lead is often effective for investigating the bioactive conformation of the lead.[14] On the other hand, a computational approach by docking simulations is also useful for investigating the noncovalent binding mode of compounds.[15] We thought that effective investigation of the noncovalent binding mode of covalent inhibitors around the transition state would be possible by combined use of the organic chemistry-based conformational restriction approach and the computational modeling.

Thus, in this report, we describe the design, synthesis, conformational analysis, and pharmacological effect of cyclopropylic strain-based conformationally restricted analogues **3b**−**5b** and **3c**−**5c** (Figure 6) and docking simulations of them and their parent compounds **3a**−**5a** to identify the noncovalent binding mode of these covalent proteasome inhibitors around the transition state. We present a useful docking concept for simulation of the noncovalent binding mode of covalent inhibitors around the transition state. On the basis of this concept, we investigated the correlation between the calculated binding energies of the simulated noncovalent complexes and the actual inhibitory effects of a series of covalent proteasome inhibitors to show that the obtained noncovalent binding mode of covalent inhibitors around the transition state can be well related to their inhibitory potency.

■ RESULTS AND DISCUSSION

Cyclopropylic Strain-Based Design of the Conformationally Restricted Analogues. Because of its small and rigid ring structure, cyclopropane is effective for restricting the conformation of a molecule without changing the chemical and

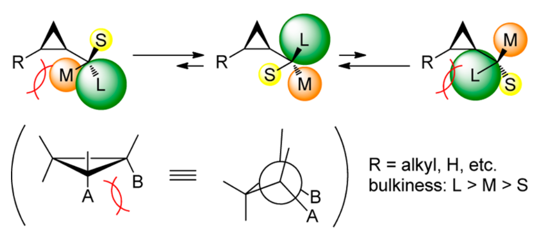

Figure 7. The cyclopropylic strain-based conformational restriction.

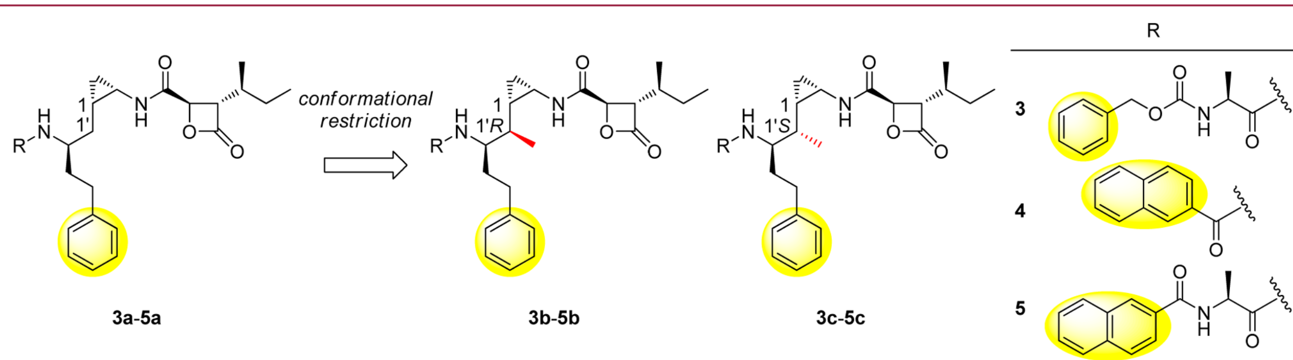

Figure 6. Previously reported proteasome inhibitors **3a**−**5a** and their conformationally restricted analogues **3b**−**5b** and **3c**−**5c**.

dx.doi.org/10.1021/jm400542h | J. Med. Chem. 2013, 56, 5829−5842

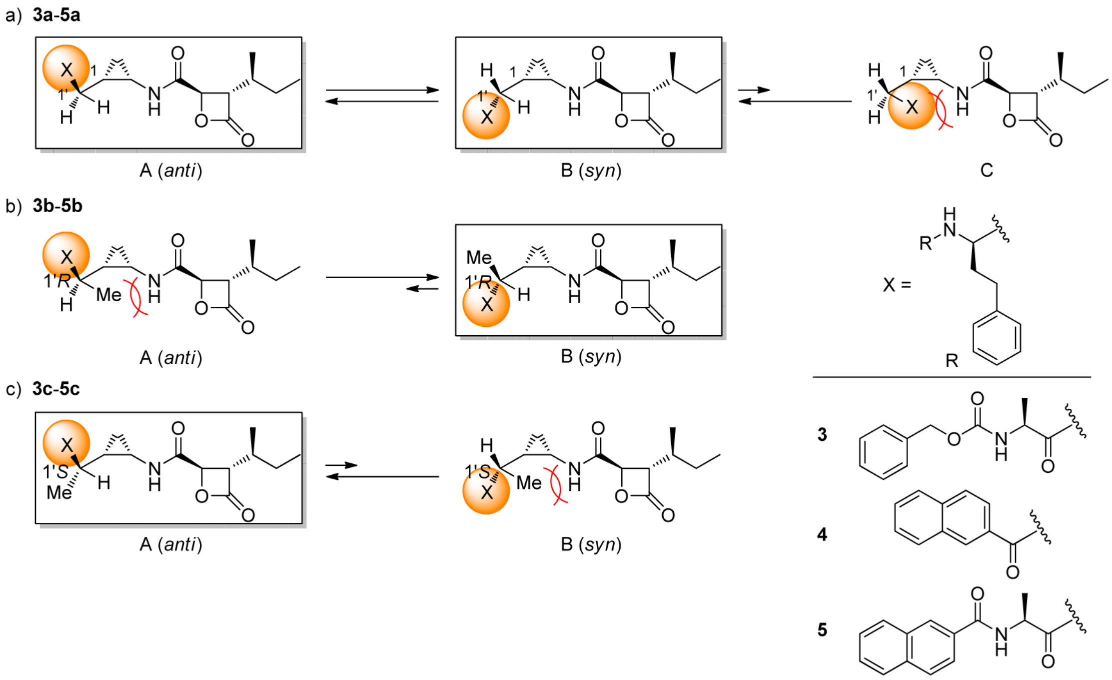

Figure 8. Plausible stable conformations of **3a**−**5a** (a), **3b**−**5b** (b), and **3c**−**5c** (c).

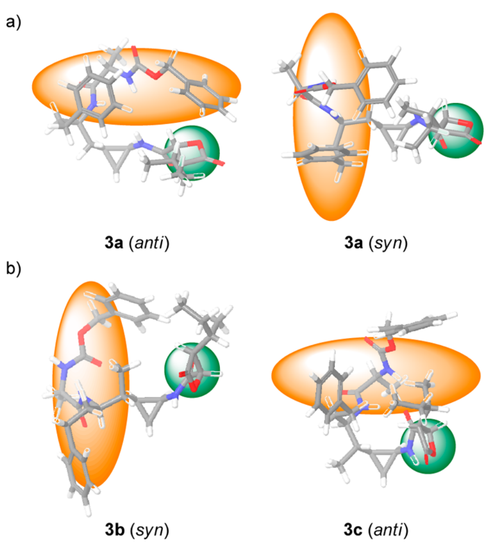

Figure 9. Stable conformations of **3a** and its conformationally restricted analogues **3b** and **3c** obtained by calculations: orange, the region containing two hydrophobic moieties; green, the β-lactone moiety.

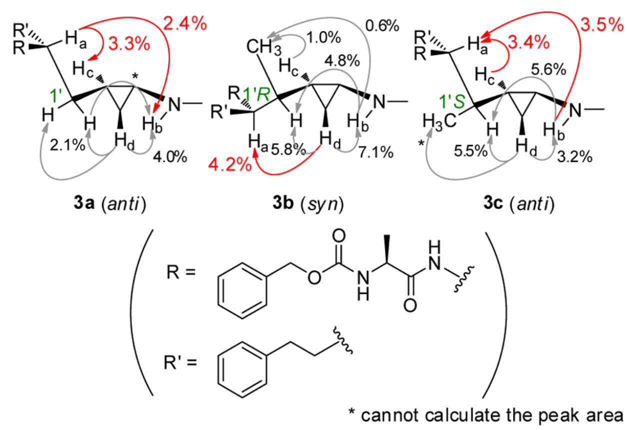

Figure 10. NOE of conformationally restricted analogues **3b** and **3c** and their parent compound **3a** in $CHCl_3$.

physical properties of the lead compound.[16] A characteristic structural feature of cyclopropane is that *cis*-oriented adjacent substituents on the ring exert significant mutual steric repulsion because they are fixed in the eclipsed orientation, which we previously termed "cyclopropylic strain".[17] Consequently, conformation of the substituents on a cyclopropane can be restricted so that the steric repulsion due to the strain is minimal, as indicated in Figure 7.

In compounds **3a**−**5a**, bond rotation between the cyclopropane (C1) and its adjacent carbon (C1′) would be restricted by the cyclopropylic strain. Thus, the two conformers A (*anti*, the cyclopropane ring "down"/the side chain (X) "up") and B (*syn*, the cyclopropane ring "down"/the side chain (X) "down") would be preferable to conformer C due to the significant steric repulsion with the adjacent *cis*-oriented amide moiety in conformer C (Figure 8a). Importantly, in the preferable conformers A (*anti*) and B (*syn*), the positioning of the side chain containing two hydrophobic moieties (X) that are essential for the strong binding to proteasome is significantly different each other, so that one of the two conformers is thought to be the bioactive form in the noncovalent complex around the transition state.

To analyze the bioactive conformation of **3a**−**5a** in the noncovalent complex around the transition state, we designed the C1′-methyl-substituted derivatives **3b**−**5b** and **3c**−**5c** as conformationally restricted analogues of **3a**−**5a** (Figure 6). Depending on the configuration at the C1′ position, conformation of the compounds can be restricted due to the cyclopropylic strain between the introduced methyl group and the *cis*-oriented amide moiety; the *syn*-conformer would be stable in **3b**−**5b** (1′*R*, Figure 8b); conversely, the *anti*-conformer would be stable in **3c**−**5c** (1′*S*, Figure 8c). Pharmacological evaluations of these conformationally restricted analogues would allow us to clarify the bioactive conformation because the analogues restricted in the bioactive conformation would be active as their

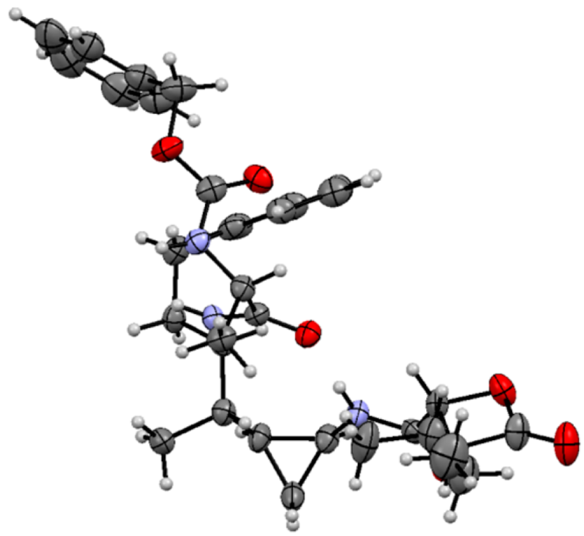

Figure 11. X-ray crystal structure of **3c**.

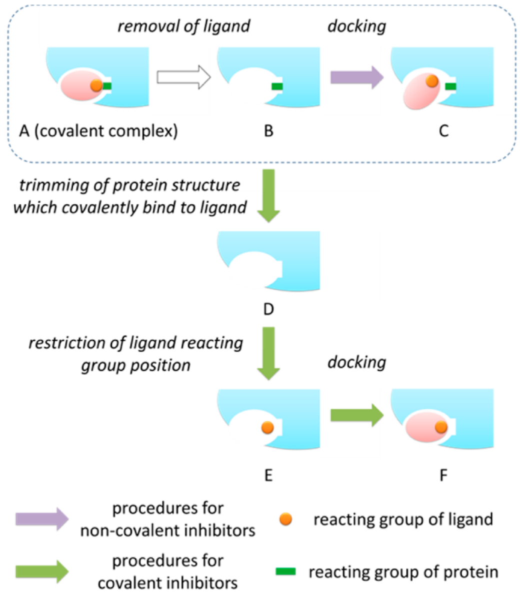

Figure 12. The concept of the docking simulation of covalent inhibitors performed by us.

parent compounds, while the analogues restricted in the different conformation would be not.

The conformations of **3a−c** were analyzed by molecular mechanics calculations with MacroModel 9.9 (Schrödinger, LLC). In the conformational analysis of **3a**, two types of particularly stable conformers were obtained, which correspond to the *anti*- and the *syn*-conformers in Figure 8a, respectively (Figure 9a), while the *anti*-conformer is slightly more stable than the *syn*-conformer (ΔE = 1.2 kcal/mol). In these two calculated conformers, positioning of the side chain containing two hydrophobic moieties (orange) relative to its *β*-lactone moiety (green) differs significantly. On the other hand, in the conformational analysis of **3b** and **3c**, the most stable structure was calculated as a *syn*-conformer for **3b** and an *anti*-conformer for **3c**, as expected (Figure 9b). The energy difference between the two conformers was rather large, which were 2.4 kcal/mol for **3b** and 7.1 kcal/mol for **3c**. The calculations of **4a−c** and **5a−c** were also carried out, and the results were similar to those for **3a−c** (see Supporting Information).

Thus, conformational analysis by molecular mechanics calculations supported our molecular design of the conformationally restricted analogues based on the cyclopropylic strain. We therefore synthesized these conformationally restricted analogues to analyze the bioactive conformation of their parent compounds in the noncovalent complex around the transition state.

Conformational Analysis of the Conformationally Restricted Analogues. We investigated the stable conformations of the synthesized conformationally restricted 1′*R* and 1′*S*-methyl derivatives **3b** and **3c** and their parent compound **3a** in $CDCl_3$ by NOE experiments (Figure 10). Irradiation of H_d of the 1′*R* isomer **3b** gave NOE at H_a, suggesting that it is stable in its *syn*-conformation. On the other hand, irradiation of H_b and H_c of the 1′*S* isomer **3c** gave NOEs at H_a, suggesting that it is stable in its *anti*-conformation. Furthermore, irradiation of H_a of the parent compound **3a**, without methyl group, gave NOEs at both H_b and H_c, suggesting that it might be rather stable in its *anti*-conformation.

We successfully analyzed the X-ray crystal structure of **3c**, which unambiguously showed its *anti*-conformation in the solid state, as expected (Figure 11).

These experimental results suggested that the conformationally restricted analogues **3b−5b** and **3c−5c** are actually stable in the conformations predicted by molecular mechanics calculations and that the cyclopropylic strain-based conformational restriction strategy seems to work effectively in these compounds, as we expected. Therefore, pharmacological evaluations of these compounds would allow us to identify the bioactive conformation of **3a−5a** in the noncovalent complex around the transition state.

Pharmacological Effects of the Conformationally Restricted Analogues. The inhibitory effects of synthesized conformationally restricted analogues **3b−5b** and **3c−5c** on the chymotrypsin-like (ChT-L) activity of purified human 20S proteasome were investigated using succinyl-Leu-Leu-Val-Tyr-4-methylcoumaryl-7-amide as a substrate (Table 1). These conformationally restricted analogues showed proteasome inhibitory activity weaker than that of their parent compounds without a methyl group at C1′. In all the C1′-stereoisomeric pairs (**3b**/**3c**, **4b**/**4c**, and **5b**/**5c**), however, the 1′*R*-isomer is significantly more potent than the corresponding 1′*S*-isomer. Therefore, the bioactive conformation of **3a−5a** in the noncovalent complex around the transition state should be the *syn*-form. The decreased activity of the 1′*R*-isomers compared with their parent compounds might be explained by steric repulsion between the introduced methyl group and proteasome.

The cell growth inhibitory effects of **3a** and its conformationally restricted analogues **3b** and **3c** against several tumor cells were also investigated. Cell growth inhibitory activity of **3c**, whose conformation is restricted in the *anti*-form, was lower than that of the parent compound **3a**, consistent with its unambiguously lower proteasome inhibitory effect than **3a**. However, the cell growth inhibitory activity of **3b**, whose conformation is restricted in the *syn*-form, is similar or even higher than that of its parent compound **3a** in all cell lines examined despite its lower proteasome inhibitory activity compared with **3a**.

To investigate these contradictory results, we focused on the stability of **3a−3c** in aqueous medium. Because these compounds were almost insoluble in water, we removed their Cbz group to obtain the water-soluble analogues **6a−6c**, respectively, for the stability evaluations. The compounds **6a−6c** were incubated in 0.1 M TEAA buffer (pH 7.4) or human AB serum at

dx.doi.org/10.1021/jm400542h | J. Med. Chem. 2013, 56, 5829−5842

Table 1. Proteasome and Cell Growth Inhibitory Effects of Conformationally Restricted Analogues 3b−5b and 3c−5c and their parent compounds 3a−5a

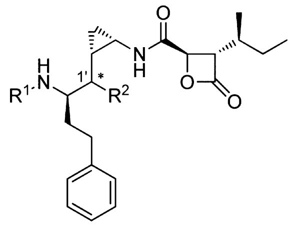

compound number	R^1	R^2	conformation	proteasome IC_{50} (nM)[a] ChT-L activity	cell growth IC_{50} (μM)[a] Hs-Sultan	KB	HCT116
3a	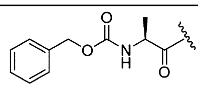			5.7 ± 1.2	0.87	2.6	1.8
4a	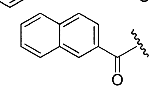	H	*syn/anti*	33 ± 8.4			
5a	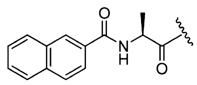			10 ± 1.0			
3b	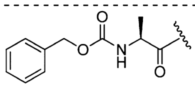			47 ± 2.9	0.31	1.7	0.63
4b	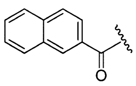	*R*-CH_3	*syn*	140 ± 36			
5b	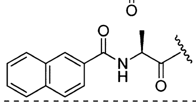			42 ± 5.8			
3c	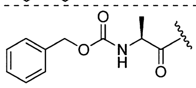			280 ± 85	1.8	> 10	> 10
4c	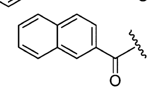	*S*-CH_3	*anti*	750 ± 100			
5c	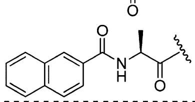			630 ± 47			
belactosin A				1440			

[a]Based on three experiments.

37 °C, and the time courses were analyzed by HPLC to obtain the half-life ($t_{1/2}$) as summarized in Table 2. Interestingly, both chemical and biological stabilities of the conformationally restricted analogues **6b** and **6c** are superior to those of their parent compound **6a**. Thus, although the proteasome inhibitory activity of conformationally restricted analogue **3b** was lower than its parent compound **3a**, the increased stability of **3b** might make it a more effective cell growth inhibitor than **3a**. The decreased structural flexibility of the compounds by the conformational restriction might be related to the increased stability.

Docking Study of 3a−3c. As described above, the noncovalent binding mode of the covalent inhibitors, especially around the transition state to form a covalent bond, can be used effectively toward designing compounds for further optimization. In the case of belactosin derivatives, the strained *β*-lactone moiety reacts with the hydroxyl group of the *N*-terminal Thr of the proteasome, which would lead to a significant conformational change of the compound via its *β*-lactone ring-opening.[10] Consequently, although the X-ray crystal structure of **3a** covalently complexed with proteasome is available, its noncovalent binding mode around the transition state could not be effectively predicted from the X-ray analysis. To investigate the noncovalent binding mode of **3a** around the transition state, we planned to perform docking simulations of **3a** and its conformationally restricted analogues **3b** and **3c**, according to the scheme shown in Figure 12.

Table 2. Half-life ($t_{1/2}$) of 6a−6c in 0.1 M TEAA Buffer (pH 7.4) or Human AB Serum at 37 °C Investigated by HPLC Analysis

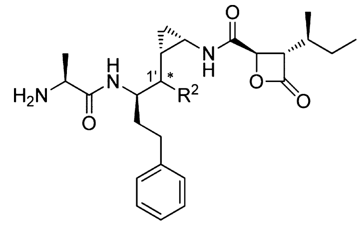

compd no.	R^2	conformation	$t_{1/2}$ 0.1 M TEAA buffer (h)	$t_{1/2}$ human AB serum (min)
6a	H	*syn/anti*	10	2.3
6b	*R*-CH_3	*syn*	14	4.2
6c	*S*-CH_3	*anti*	21	4.7

In the noncovalently interacting state of a covalent inhibitor and its target protein around the transition state to form a covalent bond, the two atoms to react each other in the inhibitor and the protein should locate closer than the sum of their van der Waals radii. Because docking programs simulate the "noncovalent interaction" (P·I in Figure 1) between the ligand and protein, they cannot simulate the binding mode including such quite close interactions around the reaction transition state (P···I in Figure 1). Therefore, if we perform docking simulations of covalent inhibitors as in the case of noncovalent inhibitors using the protein structure (B in Figure 12), in which the covalently bound inhibitor is simply removed from the X-ray crystal structure of the covalent complex (A in Figure 12), it should only produce noncovalent binding mode far from its transition state (C in Figure 12). Thus, to predict the noncovalent binding mode of **3a** around the transition state, we devised a docking method through steps B−F, depicted in Figure 12. First, the reacting group of the protein is removed to avoid steric repulsion to simulate the noncovalent complex around the transition state (B−D). Then, the plausible position of the ligand's reacting group (orange closed circle in Figure 12) in the noncovalent complex around the transition state is hypothesized based on the X-ray crystal structure of the covalent complex (A), which can be effectively used to restrict the positioning of ligand reacting group in docking simulations (D−E). The constructed model (E) consists of the trimmed protein with constraint on the ligand reacting group position would be useful to simulate the noncovalent binding mode around the transition state (E−F).

To perform the docking simulations of belactosin derivatives according to the scheme, reasonable positioning of the reacting group β-lactone is needed. However, as mentioned above, belactosin derivatives react with the proteasome Thr residue via its strained β-lactone ring-opening, which would induce significant conformational change of the belactosin derivatives[10] (Figure 13a). Accordingly, positioning of the β-lactone moiety in the noncovalent complex around the transition state is difficult to predict exactly based on the covalent complex structure. Thus, in the docking simulation of belactosin derivatives, construction of the model structure used for docking simulation (Figure 12E) based on the X-ray crystal structure (Figure 12A) is problematic.

To resolve the problem, we focused on the X-ray crystal structure of fluorosalinosporamide A covalently complexed with the proteasome.[18] Salinosporamide A and its derivatives are

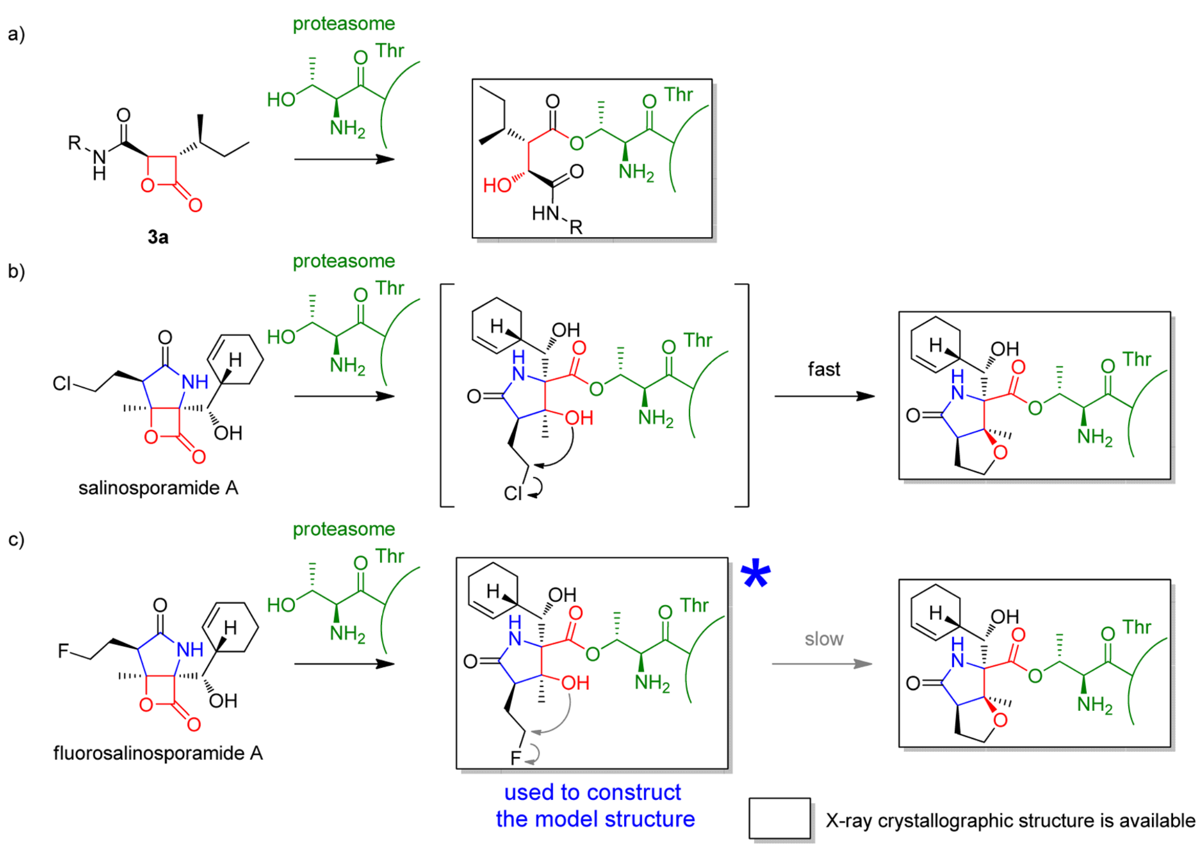

Figure 13. Inhibitory mechanism of **3a** (a), salinosporamide A (b), and fluorosalinosporamide A (c).

dx.doi.org/10.1021/jm400542h | J. Med. Chem. 2013, 56, 5829−5842

covalent inhibitors of proteasome that have a β-lactone ring as a reacting group like belactosin derivatives,[19] so that the β-lactone ring of salinosporamide seems to occupy a space similar to that occupied by belactosin derivatives in their noncovalent binding state around the transition state. Importantly, in comparison with belactosin derivatives, the conformational change of the salinosporamide derivatives induced by the β-lactone ring-opening should not be so significant because the β-lactone of salinosporamide A derivatives is fused with a γ-lactam to restrict the conformational change of the β-lactone region by the ring-opening[19c] (Figure 13b,c). In the case of salinosporamide A, after the β-lactone ring-opening reaction with the proteasome Thr residue, the resulting hydroxyl group substitutes the chloride on its chloroethyl side chain to form the five-membered ether ring,[19c] which would further differentiate its structure from that in the transition state (Figure 13b). Fortunately, in the case of fluorosalinosporamide A, having a less reactive fluoroethyl group instead of a chloroethyl group, its X-ray crystal structure in complex with the proteasome without formation of the ether ring was analyzed.[18] In the structure, conformations of both the ligand and the proteasome would be rather analogous to those in the noncovalent binding state (Figure 13c*). Therefore, we thought that the structure of fluorosalinosporamide A in complex with proteasome (Figure 13c*) would be effectively used to construct the model structure (corresponding to Figure 12E) for the docking simulations to investigate the noncovalent complex around the transition state.

Thus, as shown in Figure 14, we modified the X-ray crystallographic structure of fluorosalinosporamide A in complex with proteasome (Figure 14a)[18] to construct the model structure used for docking simulation of **3a**–**3c**. First, the ester bond between the fluorosalinosporamide A and the Thr was cleaved, and then, the side-chain of Thr was trimmed to remove the steric repulsion between the Thr side-chain and the β-lactone of **3a**–**3c** (Figure 14b).[20] Next, we reconstructed the β-lactone structure by ligating the hydroxyl oxygen and the carbonyl carbon, which was minimized by molecular mechanics calculation to give the putative noncovalent binding mode of the fluorosalinosporamide A around the transition state (Figure 14c). From the reconstructed structure of fluorosalinosporamide A, moieties other than the β-lactone ring were removed to obtain the model structure used for docking simulation, which consists of the trimmed proteasome structure and the β-lactone ring used as a core structure to restrict the β-lactone positioning of the ligand in docking simulations (Figure 14d). Thus, in this model, it is hypothesized that the reacting β-lactone is located at the position near to that in the transition state.

Using the model, we carried out the docking simulation of **3a**–**3c** to predict their noncovalent binding state around their transition states, and the results are shown in Figure 15. The predicted noncovalent binding mode of **3a** was the *syn*-form (Figure 15a) in accord with the experimental results of **3a**–**3c** described above, suggesting that the docking simulation is reliable. As expected, the predicted noncovalent binding mode of **3a** around the transition state was significantly different from the X-ray analyzed covalent binding mode (Figure 3), especially in the region containing the two hydrophobic moieties essential for its strong proteasome inhibition. Furthermore, the two aromatic groups and proteasome surface were very close to be accommodated precisely in the binding site, compared with those in the X-ray analyzed covalent complex, which further supports our hypothesis that the two hydrophobic moieties effectively interact with proteasome in the noncovalent complex

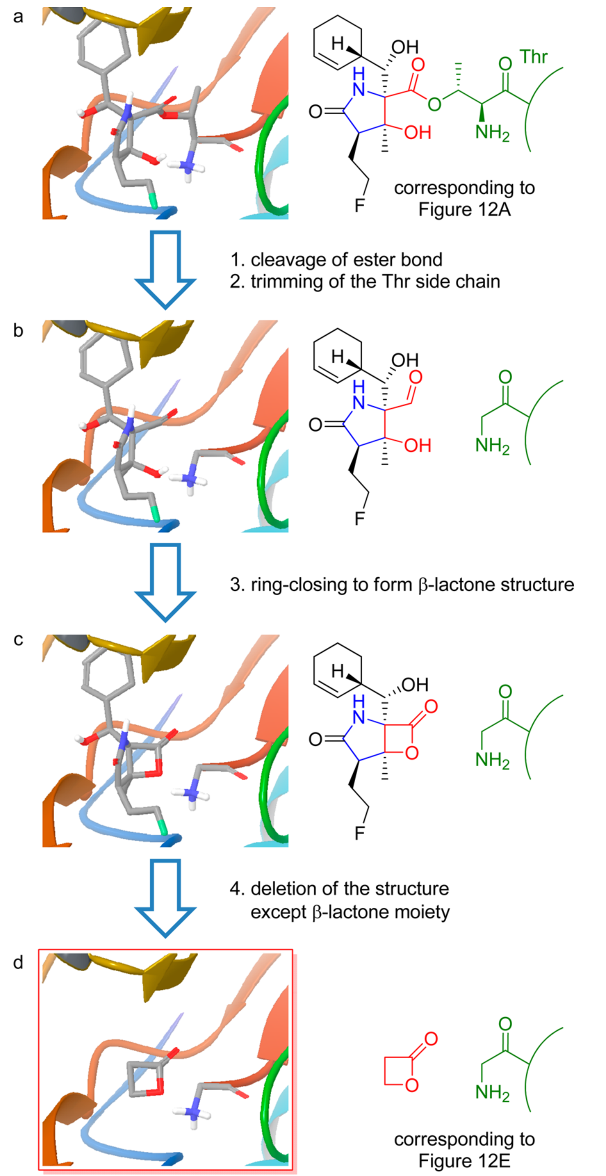

Figure 14. Modification of the X-ray crystallographic structure of the fluorosalinosporamide A in complex with proteasome.

around the transition state rather than in the covalent complex, as shown in Figure 5.

The predicted noncovalent binding mode of **3b** (Figure 15b) around the transition state was also the *syn*-form, and the region containing the two hydrophobic moieties interacts with proteasome almost the same as in **3a** (Figure 15d). On the other hand, in the docking simulation of **3c** (Figure 15c), none of plausible binding modes similar to that of **3a** was obtained. These docking results of **3b** and **3c** are consistent with their proteasome inhibitory activity, which again indicates that the docking simulation was performed properly.

Correlation between Calculated Energy of the Noncovalent Complex and Inhibitory Activity. As mentioned above, it is important to know the noncovalent binding mode around the transition state for the effective optimization of covalent inhibitors, because the inhibitory activity of covalent inhibitors can be related to the binding energy of the noncovalent complex around the transition state. On the basis of this hypothesis, we performed docking simulations of a series of salinosporamide A derivatives

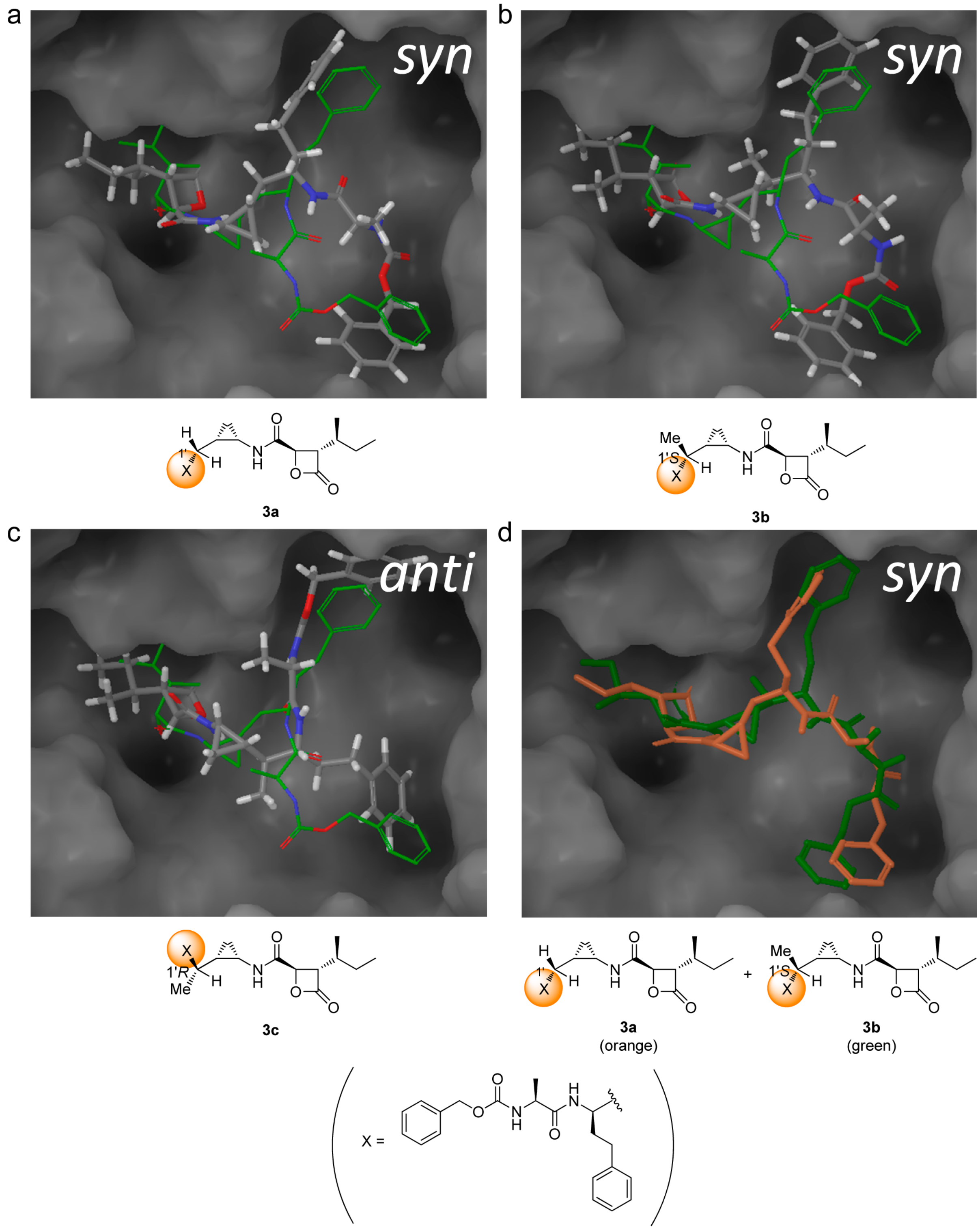

Figure 15. (a−c) The noncovalent binding mode of **3a**−**3c** around the transition state predicted by docking simulations: gray tube, predicted binding mode of each compound; green wire, structure of **3a** in covalent complex analyzed by X-ray crystallography. (d) Superimposed predicted structures of **3a** (orange tube) and **3b** (green tube).

using the proteasome model constructed in this study and calculated the binding energy of the predicted noncovalent complexes around the transition state by Prime MM-GBSA.[21] In this trial, 11 salinosporamide A derivatives, for which the IC_{50} values for yeast 20S proteasome were reported previously,[22] were used, and the correlation between their pIC_{50} and the calculated Prime MM-GBSA ΔG bind was investigated.

As shown in Figure 16a, calculated binding energies of the predicted noncovalent complexes around the transition state are well correlated to their pIC_{50} values ($r = 0.82$). Because each of these derivatives has different hydrophobic residues (see Supporting Information Figure S6), we further investigated the correlation between clogP and pIC_{50} of them (Figure 16b). However, no correlation was observed between them ($r = 0.096$),

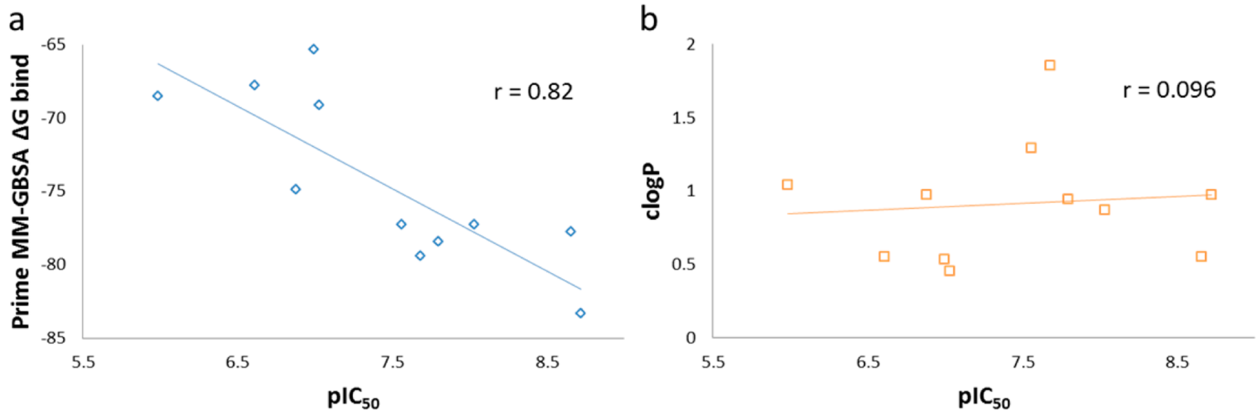

Figure 16. Calculated prime MM-GBSA Δ*G* bind vs pIC_{50} (a) and clogP vs pIC_{50} (b) of salinosporamide A derivatives.

Scheme 1. Synthetic Plan of 3b−5b

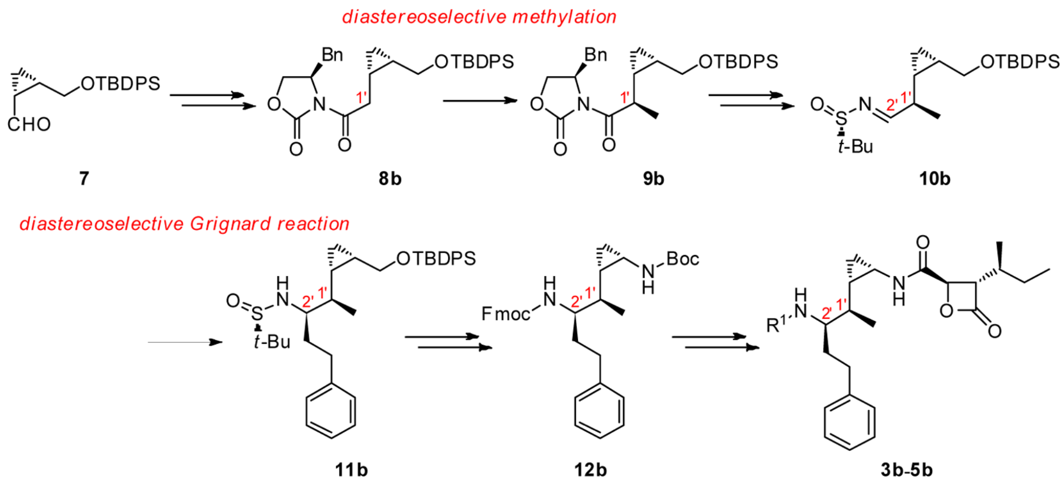

which clearly suggests that the calculated binding energies in the predicted noncovalent complexes around the transition state does not reflect the hydrophobicity of the inhibitors but effectively reflects specific hydrophobic interactions between the protein and inhibitors around the transition state. To our knowledge, this is the first demonstration of the good correlation between the inhibitory activities of covalent inhibitors and the calculated binding energies of predicted noncovalent complexes around the transition state by docking simulations.

Chemistry. The synthetic plan for **3b−5b** is summarized in Scheme 1. In the synthesis, construction of the sequential tertiary chiral carbons (C1′ and C2′) is a key. The C2′ chiral center is thought to be constructed by Grignard reaction with the sulfinylimine **10b**, as we reported previously for the synthesis of **3a−5a**.[12b] The sulfinylimine **10b** is prepared from the conformationally restricted chiral cyclopropane unit **9b**. The C1′ chiral center of **9b** seemed to be constructed by the stereoselective methylation by chiral oxazolidinone method[23] using substrate **8b**. Starting from chiral cyclopropane unit **7**, developed by us as a chiral cyclopropane unit for the synthesis of stereochemically diverse cyclopropane compounds,[24] substrate **8b** is prepared. Similarly, their diastereomers **3c−5c** are prepared (see Supporting Information about the synthesis of **3c−5c**).

Synthesis of the unit **10b** and the key intermediate **12b** are shown in Scheme 2. Cyclopropane unit **7** was subjected to a Wittig reaction with $MeOCH_2PPh_3Cl$, and subsequent hydrolysis of the product gave its homologous aldehyde, of which Pinnick oxidation afforded the corresponding carboxylic acid **13**. Condensation of **13** and (4*R*)-4-benzyl-2-oxazolidinone[23] with the mixed acid anhydride method was carried out to form **8b** to regulate the stereochemistry of the following methylation of the *α*-position (C1′) to the carbonyl group. Thus, **8b** was treated with CH_3I/NaHMDS in THF at −78 °C to stereoselectively afford the desired methylated product **9b** (dr 97:3). The undesired diastereomer was removed at the purification step of **15b** to afford it as a single diastereomer. The chiral auxiliary was removed reductively with DIBAL to yield the corresponding aldehyde **14b**, condensation of which with (*S*)-*t*-$BuSONH_2$[25] gave the conformationally restricted chiral cyclopropane unit **10b**. The absolute configuration of the introduced methyl group was determined by the PGME method[26] (see Supporting Information).

Grignard reaction of **10b** with phenethylmagnesium chloride afforded the alkylated product diastereoselectively.[25] The absolute configuration of the introduced phenethyl group was determined by the modified Mosher's method[27] (see Supporting Information). The *t*-butylsulfinyl group and TBDPS group were then removed under acidic conditions in methanol, and the resulting amino group was protected with an Fmoc group to afford **15b**. Successive oxidations of **15b** under Dess−Martin and Pinnick oxidation conditions gave the corresponding carboxylic acid, and subsequent treatment of it with DPPA gave the corresponding acyl azide, which was heated in *t*-BuOH to form the Curtius rearrangement product **12b** as a key intermediate.

Scheme 2. Synthesis of the Conformationally Restricted Chiral Cyclopropane Unit 10b and the Key Intermediate 12b[a]

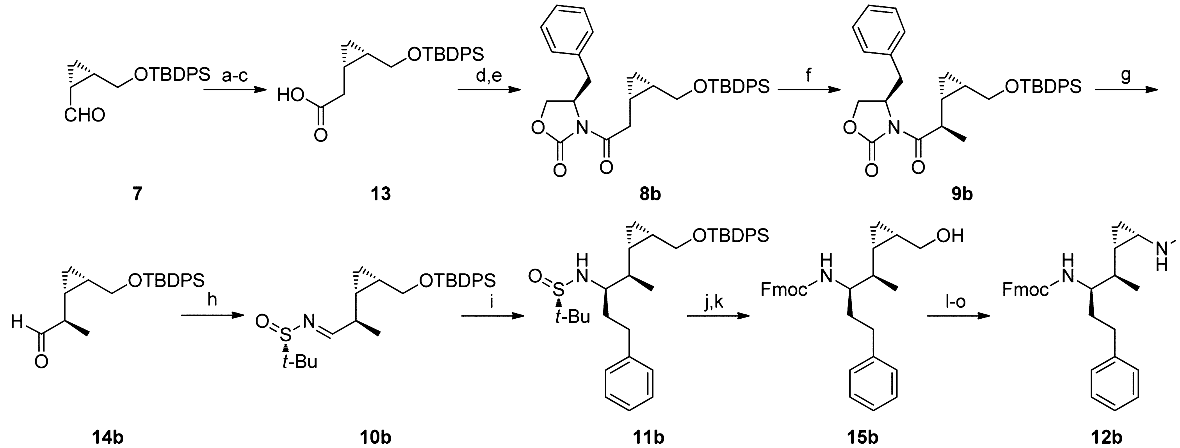

[a]Reagents and conditions: (a) $MeOCH_2PPh_3Cl$, NaHMDS, THF, 0 °C; (b) HCl, THF/H_2O; (c) Pinnick ox, 90% (3 steps from **7**); (d) PivCl, Et_3N, CH_2Cl_2, 0 °C; (e) (4*R*)-4-benzyl-2-oxazolidinone, *n*-BuLi, THF, −78 °C, 83% (2 steps from **13**); (f) CH_3I, NaHMDS, THF, −78 °C, 83% (dr 97:3); (g) DIBAL, THF, −78 °C, 69%; (h) (*S*)-*t*-$BuSONH_2$, $CuSO_4$, CH_2Cl_2, 96%; (i) $PhCH_2CH_2MgCl$, CH_2Cl_2; (j) HCl, AcOEt/MeOH; (k) FmocOSu, Na_2CO_3, THF/H_2O, 66% (3 steps from **10b**); (l) Dess−Martin ox; (m) Pinnick ox; (n) DPPA, Et_3N, CH_2Cl_2, 0 °C to rt; (o) *t*-BuOH, reflux, 72% (4 steps from **15b**).

Scheme 3. Synthesis of 3b−5b[a]

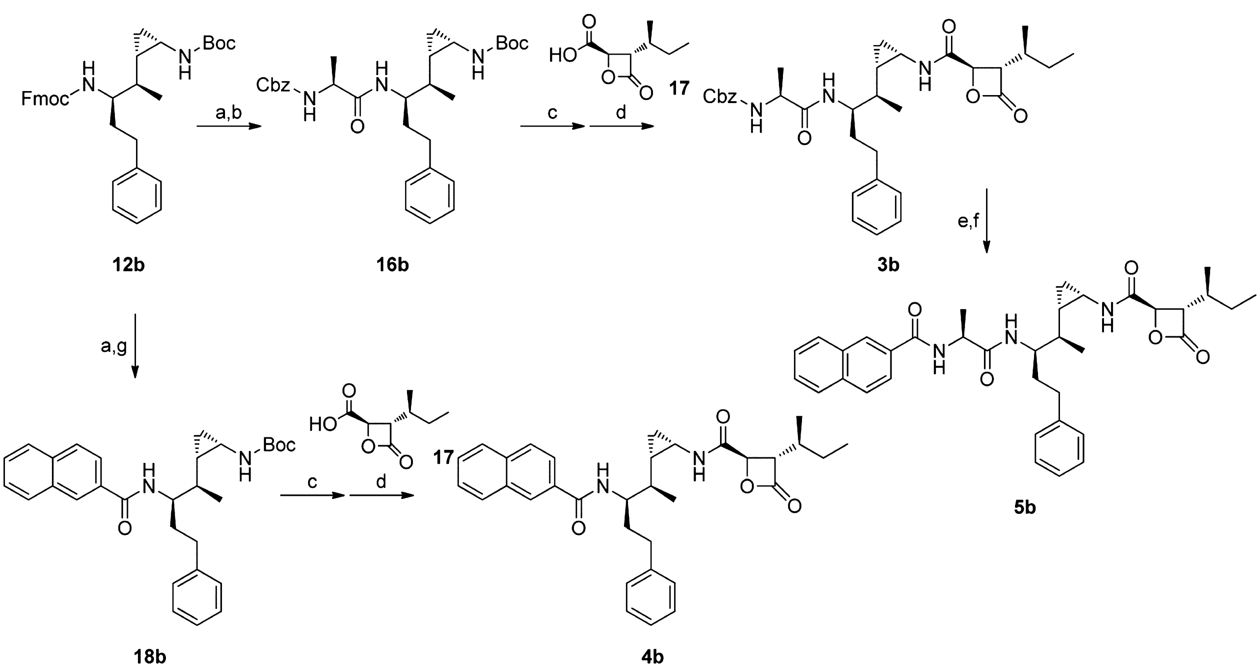

[a]Reagents and conditions: (a) K_2CO_3, MeOH; (b) Cbz-Ala-OPiv, Et_3N, CH_2Cl_2, 0 °C to rt, 100% (2 steps from **12b**); (c) TFA/CH_2Cl_2; (d) PivCl, Et_3N, CH_2Cl_2, 0 °C to rt, (**3b**, two steps 82% from **16b**; **4b**, two steps 91% from **18b**); (e) Pd/C, H_2, TFA/THF, 0 °C; (f) 2-naphthoyl chloride, Et_3N, CH_2Cl_2, 0 °C, 70% (2 steps from **3b**); (g) 2-naphthoyl chloride, Et_3N, CH_2Cl_2, 0 °C, 100% (2 steps from **12b**).

The synthesis of **3b**−**5b** is shown in Scheme 3. After removal of the Fmoc group of **12b** with K_2CO_3 in methanol, Cbz-Ala-OH was condensed with the mixed anhydride method to yield **16b**. After removal of the Boc group of **16b** with TFA in DCM, the β-lactone unit **17**[28] was condensed by the mixed anhydride method to yield **3b**. The Cbz group of **3b** was removed by hydrogenolysis, and the product was treated with 2-naphthoyl chloride to afford **5b**. Compound **4b** was prepared from **12b** as the preparation of **3b**.

During these synthetic studies, we observed that the diastereoselectivity of the Grignard reactions of **10b** and **10c** was significantly affected by the configuration of the C1′ methyl group adjacent to the imino moiety. In these reactions, the 1′*R* substrate **10b** gave **11b** as a single isomer, while the 1′*S* substrate **10c** gave **11c** as a diastereomeric mixture in a ratio of 5:1. The different stereochemical outcome between these substrates might be explained by the reaction mechanism shown in Figure 17. The Grignard reaction of the *t*-butylsulfinylimines is thought to proceed through a six-membered transition state due to coordination of the sulfinyl oxygen to the Mg^{2+}, in which the bulky *t*-butyl group is in the equatorial position to determine the stereochemistry of the reaction (Ellman model).[25] When the substrate is the 1′*S* isomer **10c**, the methyl group adjacent to the imino moiety should be

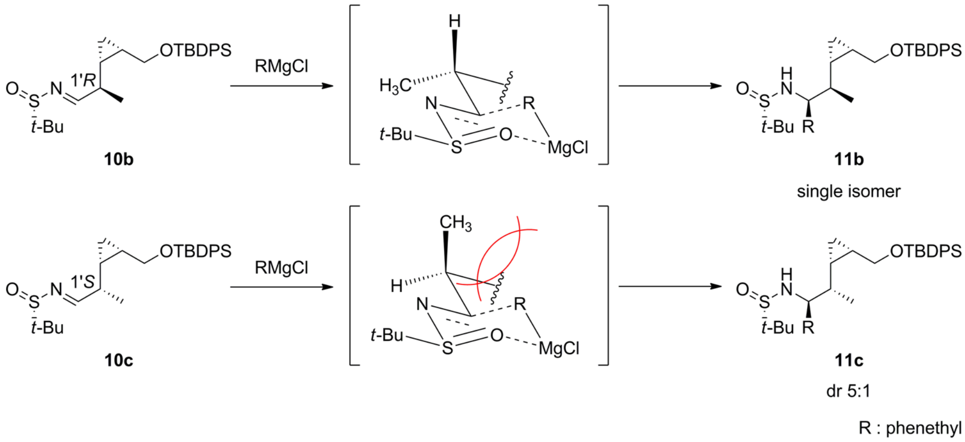

Figure 17. Plausible reaction mechanisms of diastereoselective Grignard reactions.

positioned on the reagent-accessible side of the imine plane in the Ellman model, and therefore, its steric effect might lower the stereoselectivity.

■ CONCLUSIONS

We successfully analyzed the noncovalent binding mode of **3a** with proteasome around the transition state using both a conformational restriction approach based on the cyclopropylic strain and docking simulations. Although precise prediction of the noncovalent binding mode of covalent inhibitors around the transition state based on X-ray crystallographic analysis is often unsuccessful, our findings suggest that the combined use of a conformational restriction approach and docking simulations can be effective to investigate the noncovalent binding mode of covalent inhibitors around the transition state in various cases. Furthermore, we calculated the binding energy of a series of salinosporamide derivatives in the predicted noncovalent complex around the transition state with the simulation model of proteasome constructed in this study, and the results are well correlated to the pIC_{50}. These findings indicate that the noncovalent binding mode around the transition state can be a key in the binding between covalent inhibitors and their target molecules. Thus, reliable docking methods to predict the noncovalent binding mode of covalent inhibitors around the transition state can be helpful toward the development of potent covalent inhibitors, and an organic chemistry approach by the conformational restriction is very effective to verify the simulation results.

■ ASSOCIATED CONTENT

Supporting Information

Experimental details of synthesis, stability testing, biological evaluations, computational simulations, and a table listing combustion analysis data for target compounds. This material is available free of charge via the Internet at http://pubs.acs.org.

■ AUTHOR INFORMATION

Corresponding Author

*Phone/Fax: +81-11-706-3769. E-mail: shu@pharm.hokudai.ac.jp. Address: Faculty of Pharmaceutical Sciences, Hokkaido University, Kita-12, Nishi-6, Kita-ku, Sapporo 060-0812, Japan.

Notes

The authors declare no competing financial interest.

■ ACKNOWLEDGMENTS

This investigation was supported by Grant-in-Aids for Scientific Research (21390028) from the Japan Society for the Promotion of Science.

■ ABBREVIATIONS USED

Boc, *tert*-butoxycarbonyl; Cbz, benzyloxycarbonyl; ChT-L, chymotrypsin-like; DIBAL, diisobutylaluminium hydride; DCM, dichloromethane; DPPA, diphenylphosphoryl azide; ERAD, endoplasmic reticulum-associated protein degradation; Fmoc, 9-fluorenylmethyloxycarbonyl; MM-GBSA, molecular mechanics generalized Born surface area; PGME, phenylglycine methyl ester; Piv, pivaloyl; TBDPS, *tert*-butyldiphenylsilyl; TEAA, triethylammonium acetate

■ REFERENCES

(1) (a) Singh, J.; Petter, R. C.; Baillie, T. A.; Whitty, A. The resurgence of covalent drugs. *Nature Rev. Drug Discovery* **2011**, *10*, 307−317. (b) Smith, A. J.; Zhang, X.; Leach, A. G.; Houk, K. N. Beyond picomolar affinities: quantitative aspects of noncovalent and covalent binding of drugs to proteins. *J. Med. Chem.* **2009**, *52*, 225−233. (c) Potashman, M. H.; Duggan, M. E. Covalent Modifiers: An Orthogonal Approach to Drug Design. *J. Med. Chem.* **2009**, *52*, 1231−1246.

(2) Evans, M. J.; Cravatt, B. F. Mechanism-Based Profiling of Enzyme Families. *Chem. Rev.* **2006**, *106*, 3279−3301.

(3) (a) Davis, A. M.; Teague, S. J.; Kleywegt, G. J. Application and limitations of X-ray crystallographic data in structure-based ligand and drug design. *Angew. Chem., Int. Ed. Engl.* **2003**, *42*, 2718−2736. (b) Hajduk, P. J.; Greer, J. A decade of fragment-based drug design: strategic advances and lessons learned. *Nature Rev. Drug Discovery* **2007**, *6*, 211−219. (c) Congreve, M.; Langmead, C. J.; Mason, J. S.; Marshall, F. H. Progress in structure based drug design for G protein-coupled receptors. *J. Med. Chem.* **2011**, *54*, 4283−4311.

(4) (a) Adams, J. The proteasome: a suitable antineoplastic target. *Nature Rev. Cancer* **2004**, *4*, 349−360. (b) Kisselev, A. F.; van der Linden, W. A.; Overkleeft, H. S. Proteasome inhibitors: an expanding army attacking a unique target. *Chem. Biol.* **2012**, *19*, 99−115. (c) Dick, L. R.; Fleming, P. E. Building on bortezomib: second-generation proteasome inhibitors as anti-cancer therapy. *Drug Discovery Today* **2010**, *15*, 243−249. (d) Orlowski, R. Z.; Kuhn, D. J. Proteasome inhibitors in cancer therapy: lessons from the first decade. *Clin. Cancer Res.* **2008**, *14*, 1649−1657. (e) Schneekloth, J. S.; Crews, C. M. Natural Product Inhibitors of the Ubiquitin−Proteasome Pathway. *Curr. Drug Targets* **2011**, *12*, 1581−1594. (f) Myung, J.; Kim, K. B.; Crews, C. M. The ubiquitin−proteasome pathway and proteasome inhibitors. *Med. Res. Rev.* **2001**, *21*, 245−273.

(5) King, R. W.; Deshaies, R. J.; Peters, J. M.; Kirschner, M. W. How proteolysis drives the cell cycle. *Science* **1996**, *274*, 1652−1659.

(6) (a) Fuchs, S. Y. The role of ubiquitin−proteasome pathway in oncogenic signaling. *Cancer Biol. Ther.* **2002**, *1*, 337−341. (b) Chen, J. J.; Lin, F.; Qin, Z. H. The roles of the proteasome pathway in signal transduction and neurodegenerative diseases. *Neurosci. Bull.* **2008**, *24*, 183−194.

(7) (a) Vembar, S. S.; Brodsky, J. L. One step at a time: endoplasmic reticulum-associated degradation. *Nature Rev. Mol. Cell Biol.* **2008**, *9*, 944−957. (b) Ron, D.; Walter, P. Signal integration in the endoplasmic reticulum unfolded protein response. *Nature Rev. Mol. Cell Biol.* **2007**, *8*, 519−529. (c) Hiller, M. M.; Finger, A.; Schweiger, M.; Wolf, D. H. ER degradation of a misfolded luminal protein by the cytosolic ubiquitin−proteasome pathway. *Science* **1996**, *273*, 1725−1728.

(8) (a) Paramore, A.; Frantz, S. Bortezomib. *Nature Rev. Drug Discovery* **2003**, *2*, 611−612. (b) Bross, P. F.; Kane, R.; Farrell, A. T.; Abraham, S.; Benson, K.; Brower, M. E.; Bradley, S.; Gobburu, J. V.; Goheer, A.; Lee, S. L.; Leighton, J.; Liang, C. Y.; Lostritto, R. T.; McGuinn, W. D.; Morse, D. E.; Rahman, A.; Rosario, L. A.; Verbois, S. L.; Williams, G.; Wang, Y. C.; Pazdur, R. Approval summary for bortezomib for injection in the treatment of multiple myeloma. *Clin. Cancer Res.* **2004**, *10*, 3954−3964. (c) Kane, R. C.; Farrell, A. T.; Sridhara, R.; Pazdur, R. United States Food and Drug Administration approval summary: bortezomib for the treatment of progressive multiple myeloma after one prior therapy. *Clin. Cancer Res.* **2006**, *12*, 2955−2960. (d) Abraham, J. Carfilzomib and bortezomib therapy in patients with multiple myeloma. *Community Oncol.* **2012**, *9*, 278−282.

(9) (a) Asai, A.; Hasegawa, A.; Ochiai, K.; Yamashita, Y.; Mizukami, T. Belactosin A, a novel antitumor antibiotic acting on cyclin/CDK mediated cell cycle regulation, produced by Streptomyces sp. *J. Antibiot.* **2000**, *53*, 81−83. (b) Asai, A.; Tsujita, T.; Sharma, S. V.; Yamashita, Y.; Akinaga, S.; Funakoshi, M.; Kobayashi, H.; Mizukami, T. A new structural class of proteasome inhibitors identified by microbial screening using yeast-based assay. *Biochem. Pharmacol.* **2004**, *67*, 227−234.

(10) Groll, M.; Larionov, O. V.; Huber, R.; De Meijere, A. Inhibitor-binding mode of homobelactosin C to proteasomes: new insights into class I MHC ligand generation. *Proc. Natl. Acad. Sci. U. S. A.* **2006**, *103*, 4576−4579.

(11) Yoshida, K.; Yamaguchi, K.; Sone, T.; Unno, Y.; Asai, A.; Yokosawa, H.; Matsuda, A.; Arisawa, M.; Shuto, S. Synthesis of 2,3- and 3,4-methanoamino acid equivalents with stereochemical diversity and their conversion into the tripeptide proteasome inhibitor belactosin a and its highly potent *cis*-cyclopropane stereoisomer. *Org. Lett.* **2008**, *10*, 3571−3574.

(12) (a) Yoshida, K.; Yamaguchi, K.; Mizuno, A.; Unno, Y.; Asai, A.; Sone, T.; Yokosawa, H.; Matsuda, A.; Arisawa, M.; Shuto, S. Three-dimensional structure−activity relationship study of belactosin A and its stereo- and regioisomers: development of potent proteasome inhibitors by a stereochemical diversity-oriented strategy. *Org. Biomol. Chem.* **2009**, *7*, 1868−1877. (b) Kawamura, S.; Unno, Y.; List, A.; Mizuno, A.; Tanaka, M.; Sasaki, T.; Arisawa, M.; Asai, A.; Groll, M.; Shuto, S. Potent Proteasome Inhibitors Derived from the Unnatural *cis*-Cyclopropane Isomer of Belactosin A: Synthesis, Biological Activity, and Mode of Action. *J. Med. Chem.* **2013**, *56*, 3689−3700.

(13) (a) Parthasarathy, S.; Murthy, M. Protein thermal stability: insights from atomic displacement parameters (*B* values). *Protein Eng.* **2000**, *13*, 9−13. (b) Yuan, Z.; Zhao, J.; Wang, Z.-X. Flexibility analysis of enzyme active sites by crystallographic temperature factors. *Protein Eng.* **2003**, *16*, 109−114. (c) Radivojac, P.; Obradovic, Z.; Smith, D. K.; Zhu, G.; Vucetic, S.; Brown, C. J.; Lawson, J. D.; Dunker, A. K. Protein flexibility and intrinsic disorder. *Protein Sci.* **2009**, *13*, 71−80.

(14) (a) Kozikowski, A. P. *Drug Design for Neuroscience*; Raven Press: New York, 1993; (b) Silverman, R. B. *The Organic Chemistry of Drug Design and Drug Action*; Academic Press: New York, 2004. (c) Wermuth, C. G. *The Practice of Medicinal Chemistry*; Academic Press: New York, 2008.

(15) (a) Kitchen, D. B.; Decornez, H.; Furr, J. R.; Bajorath, J. Docking and scoring in virtual screening for drug discovery: methods and applications. *Nature Rev. Drug Discovery* **2004**, *3*, 935−949. (b) Taylor, R. D.; Jewsbury, P. J.; Essex, J. W. A review of protein−small molecule docking methods. *J. Comput.-Aided Mol. Des.* **2002**, *16*, 151−166.

(16) (a) Armstrong, P. D.; Cannon, J. G.; Long, J. P. Conformationally Rigid Analogues of Acetylcholine. *Nature* **1968**, *220*, 65−66. (b) Kazuta, Y.; Hirano, K.; Natsume, K.; Yamada, S.; Kimura, R.; Matsumoto, S.; Furuichi, K.; Matsuda, A.; Shuto, S. Cyclopropane-based conformational restriction of histamine. (1*S*,2*S*)-2-(2-aminoethyl)-1-(1*H*-imidazol-4-yl)cyclopropane, a highly selective agonist for the histamine H3 receptor, having a *cis*-cyclopropane structure. *J. Med. Chem.* **2003**, *46*, 1980−1988. (c) Watanabe, M.; Kazuta, Y.; Hayashi, H.; Yamada, S.; Matsuda, A.; Shuto, S. Stereochemical diversity-oriented conformational restriction strategy. Development of potent histamine H3 and/or H4 receptor antagonists with an imidazolylcyclopropane structure. *J. Med. Chem.* **2006**, *49*, 5587−5596. (d) Watanabe, M.; Kobayashi, T.; Hirokawa, T.; Yoshida, A.; Ito, Y.; Yamada, S.; Orimoto, N.; Yamasaki, Y.; Arisawa, M.; Shuto, S. Cyclopropane-based stereochemical diversity-oriented conformational restriction strategy: histamine H3 and/or H4 receptor ligands with the 2,3-methanobutane backbone. *Org. Biomol. Chem.* **2012**, *10*, 736−745.

(17) (a) Shuto, S.; Ono, S.; Hase, Y.; Kamiyama, N.; Takada, H.; Yamasihita, K.; Matsuda, A. Conformational restriction by repulsion between adjacent substituents on a cyclopropane ring: Design and enantioselective synthesis of 1-phenyl-2-(1-aminoalkyl)-*N*,*N*-diethylcyclopropanecarboxamide as potent NMDA receptor antagonists. *J. Org. Chem.* **1996**, *61*, 915−923. (b) Shuto, S.; Ono, S.; Hase, Y.; Ueno, Y.; Noguchi, T.; Yoshii, K.; Matsuda, A. Synthesis and biological activity of conformationally restricted analogs of milnacipran: (1*S*,2*R*)-1-phenyl-2-[(*S*)-1-aminopropyl]-*N*,*N*-diethylcyclopropanecarboxamide, an efficient noncompetitive *N*-methyl-D-aspartic acid receptor antagonist. *J. Med. Chem.* **1996**, *39*, 4844−4852. (c) Shuto, S.; Ono, S.; Imoto, H.; Yoshii, K.; Matsuda, A. Synthesis and biological activity of conformationally restricted analogues of milnacipran: (1*S*,2*R*)-1-phenyl-2-[(*R*)-1-amino-2-propynyl]-*N*,*N*-diethylcyclopropanecarboxamide is a novel class of NMDA receptor channel blocker. *J. Med. Chem.* **1998**, *41*, 3507−3514. (d) Ono, S.; Ogawa, K.; Yamashita, K.; Yamamoto, T.; Kazuta, Y.; Matsuda, A.; Shuto, S. Conformational analysis of the NMDA receptor antagonist (1*S*,2*R*)-1-phenyl-2-[(*S*)-1-aminopropyl]-*N*,*N*-diethylcyclopropanecarboxamide (PPDC) designed by a novel conformational restriction method based on the structural feature of cyclopropane ring. *Chem. Pharm. Bull.* **2002**, *50*, 966−968. (e) Yamaguchi, K.; Kazuta, Y.; Hirano, K.; Yamada, S.; Matsuda, A.; Shuto, S. Synthesis of 1-arylpiperazyl-2-phenylcyclopropanes designed as antidopaminergic agents: cyclopropane-based conformationally restricted analogs of haloperidol. *Bioorg. Med. Chem.* **2008**, *16*, 8875−8881. (f) Watanabe, M.; Hirokawa, T.; Kobayashi, T.; Yoshida, A.; Ito, Y.; Yamada, S.; Orimoto, N.; Yamasaki, Y.; Arisawa, M.; Shuto, S. Investigation of the bioactive conformation of histamine H3 receptor antagonists by the cyclopropylic strain-based conformational restriction strategy. *J. Med. Chem.* **2010**, *53*, 3585−3593.

(18) Groll, M.; McArthur, K. A.; Macherla, V. R.; Manam, R. R.; Potts, B. C. Snapshots of the fluorosalinosporamide/20S complex offer mechanistic insights for fine tuning proteasome inhibition. *J. Med. Chem.* **2009**, *52*, 5420−5428.

(19) (a) Feling, R. H.; Buchanan, G. O.; Mincer, T. J.; Kauffman, C. A.; Jensen, P. R.; Fenical, W. Salinosporamide A: a highly cytotoxic proteasome inhibitor from a novel microbial source, a marine bacterium of the new genus salinospora. *Angew. Chem., Int. Ed. Engl.* **2003**, *42*, 355−357. (b) Macherla, V. R.; Mitchell, S. S.; Manam, R. R.; Reed, K. A.; Chao, T. H.; Nicholson, B.; Deyanat-Yazdi, G.; Mai, B.; Jensen, P. R.; Fenical, W. F.; Neuteboom, S. T.; Lam, K. S.; Palladino, M. A.; Potts, B. C. Structure−activity relationship studies of salinosporamide A (NPI-0052), a novel marine derived proteasome inhibitor. *J. Med. Chem.* **2005**, *48*, 3684−3687. (c) Groll, M.; Huber, R.; Potts, B. C. M. Crystal structures of salinosporamide A (NPI-0052) and B (NPI-0047) in complex with the 20S proteasome reveal important consequences of beta-lactone ring opening and a mechanism for irreversible binding. *J. Am. Chem. Soc.* **2006**, *128*, 5136−5141.

(20) In the docking simulation using the native proteasome structure with positional constraint of β-lactone moiety, no pose was obtained,

probably due to significant steric repulsion between β-lactone and Thr side-chain.

(21) (a) Guimarães, C. MM-GB/SA Rescoring of Docking Poses. *Methods Mol. Biol.* **2012**, *819*, 255. (b) Guimarães, C. R. W.; Cardozo, M. MM-GB/SA Rescoring of Docking Poses in Structure-Based Lead Optimization. *J. Chem. Inf. Model.* **2008**, *48*, 958−970. (c) Lyne, P. D.; Lamb, M. L.; Saeh, J. C. Accurate Prediction of the Relative Potencies of Members of a Series of Kinase Inhibitors Using Molecular Docking and MM-GBSA Scoring. *J. Med. Chem.* **2006**, *49*, 4805−4808.

(22) (a) Nett, M.; Gulder, T. A. M.; Kale, A. J.; Hughes, C. C.; Moore, B. S. Function-oriented biosynthesis of β-lactone proteasome inhibitors in *Salinispora tropica*. *J. Med. Chem.* **2009**, *52*, 6163−6167. (b) Manam, R. R.; McArthur, K. A.; Chao, T. H.; Weiss, J.; Ali, J. A.; Palombella, V. J.; Groll, M.; Lloyd, G. K.; Palladino, M. A.; Neuteboom, S. T. C. Leaving groups prolong the duration of 20S proteasome inhibition and enhance the potency of salinosporamides. *J. Med. Chem.* **2008**, *51*, 6711−6724.

(23) Evans, D. A.; Wu, L. D.; Wiener, J. J. M.; Johnson, J. S.; Ripin, D. H. B.; Tedrow, J. S. A General Method for the Synthesis of Enantiomerically Pure β-Substituted, β-Amino Acids through α-Substituted Succinic Acid Derivatives. *J. Org. Chem.* **1999**, *64*, 6411−6417.

(24) Kazuta, Y.; Matsuda, A.; Shuto, S. Development of versatile *cis*- and *trans*-dicarbon-substituted chiral cyclopropane units: synthesis of (1*S*,2*R*)- and (1*R*,2*R*)-2-aminomethyl-1-(1H-imidazol-4-yl)-cyclopropanes and their enantiomers as conformationally restricted analogues of histamine. *J. Org. Chem.* **2002**, *67*, 1669−1677.

(25) Cogan, D. A.; Liu, G.; Ellman, J. Asymmetric synthesis of chiral amines by highly diastereoselective 1,2-additions of organometallic reagents to *N-tert*-butanesulfinyl imines. *Tetrahedron* **1999**, *55*, 8883−8904.

(26) Yabuuchi, T.; Kusumi, T. Phenylglycine methyl ester, a useful tool for absolute configuration determination of various chiral carboxylic acids. *J. Org. Chem.* **2000**, *65*, 397−404.

(27) (a) Ohtani, I.; Kusumi, T.; Kashman, Y.; Kakisawa, H. High-field FT NMR application of Mosher's method. The absolute configurations of marine terpenoids. *J. Am. Chem. Soc.* **1991**, *113*, 4092−4096. (b) Kusumi, T.; Fukushima, T.; Ohtani, I.; Kakisawa, H. Elucidation of the absolute configurations of amino acids and amines by the modified mosher's method. *Tetrahedron Lett.* **1991**, *32*, 2939−2942.

(28) Armstrong, A.; Scutt, J. N. Total synthesis of (+)-belactosin A. *Chem. Commun.* **2004**, 510−511.